



## DYNAMIC RUPTURE SIMULATIONS OF A VERTICAL STRIKE-SLIP FAULT WITH HETEROGENEOUS STRESS-DROP DISTRIBUTION

H. Kawase<sup>(1)</sup>, J. Sun<sup>(2)</sup>, A. Pitarka<sup>(3)</sup>, L. Dalguer<sup>(4)</sup>, E. Ito<sup>(5)</sup>, and F. Nagashima<sup>(6)</sup>

<sup>(1)</sup> Program-Specific Professor, DPRI, Kyoto University, kawase@sere.dpri.kyoto-u.ac.jp

<sup>(2)</sup> Ph.D. Candidate, Grad. School of Eng., Kyoto University, sun@zeisei.dpri.kyoto-u.ac.jp

<sup>(3)</sup> Seismologist, Lawrence Livermore National Laboratory, pitarka1@llnl.gov

<sup>(4)</sup> Seismologist & Structural Engineer, 3Q-LAB. GmbH, luis.dalguer@gmail.com

<sup>(5)</sup> Program-Specific Researcher, DPRI, Kyoto University, ito@sere.dpri.kyoto-u.ac.jp

<sup>(6)</sup> Program-Specific Assistant Professor, DPRI, Kyoto University, nagashima@sere.dpri.kyoto-u.ac.jp

### Abstract

We investigated here the effects of source parameters that describe the complex nature of the source rupture process, with special focus on the spatial heterogeneity of the stress drop on the fault. We considered both random fluctuations as in Pitarka et al. (2009) and two rectangular asperities where the average stress drop is twice (6.4 MPa) as large as the global one (3.2MPa). The area of asperities follows the scaling law of Irikura and Miyake (2011).

We also consider the depth dependence of the stress drop distribution outside of the major seismogenic zone to confine the major slip generation areas. Geometric parameters such as the rupture initiation point, the relative separation distance between two asperities, and the depths of the two asperities are chosen to be investigated in our parametric study. The assumed fault is a vertical strike-slip fault with the size (L x W) = (25 km x 18 km). The dynamic rupture simulations were performed by the FDM code using the split-node formulation by Dalguer and Day (2007).

First, we confirmed if the computed averaged slip and the peak ground velocity correspond to the values predicted by empirical relationships. Then we investigated the effects of  $D_c$ , asperity depths, and the stress drop distribution with the depth on the final slip distribution and resulting peak ground velocity distribution. If we put asperities in the deeper part of the fault, we could not see much of the surface rupture, while if we put two shallow asperities the resultant surface break (displacement) becomes larger. If we decrease the stress drop near the surface, such a large surface break would be no longer emerged on the surface. When we compare the case of positive stress drop near the surface with the case of negative stress drop near the surface, we can see an apparently larger slip amount in the former near the surface. At the same time even if we see large slips in the areas near the surface, the peak slip velocity in the shallower part of the fault is much smaller than those inside the asperities. Therefore, the peak ground velocity on the surface in the near-fault region is mainly controlled by the directivity in the waves generated from the asperity, not the fault slip in the shallower part of the fault. As for the effect of  $D_c$ ,  $D_c$  controlled the progress of rupture. The rupture will stop if  $D_c$  is too large.

In these parametric studies we can see how the depths of asperities and the complex stress drop distribution on the fault affect the final slip distribution and the ground motion intensity on the surface. We need to further consider the effects of the different stress drops in the asperities as a function of their depths, as seen in observations (Nakano et al., 2015). We also consider the relationships of the combined areas of SMGAs derived from our dynamic rupture simulations with respect to the combined areas of the assumed high-stress regions (asperities) to confirm the appropriateness of our model assumptions in terms of the scaling law of Irikura and Miyake (2011).

*Keywords: Dynamic rupture; Surface displacements; Near Fault Ground Motions; Stress Drop; Asperity*



## 1. Introduction

From the latter half of the 1970s, the dynamic rupture simulation of fault motions has been investigated based on fracture mechanics, starting from simple fracture problems of cracks. The initial researches were focused on reproducing the basic dynamic rupture properties, such as whether or not the rupture progresses, how the propagation speed changes when it progresses, and what is the shape of the slip velocity function in asperities, by setting the fracture parameters on simple and uniform fault rupture surfaces. Thereafter, it has been found that the nonlinear fracture behavior of the fault plane can be clearly described by a slip-weakening model, and the model can reproduce recorded near-fault ground motion characteristics. In particular, with the increase of computation power, realistic rupture simulations have become possible by setting heterogeneous fault rupture parameters, considering both the depth dependency and random fluctuations, instead of the spatial distribution of a homogeneous fault rupture parameter.

There is a limit for the amount of data available for deriving important empirical relationships, such as the relationship between the fault width and seismogenic layer, the relationship between the maximum and average slips in the seismogenic layer as well as areas near the ground surface, and the influence of coupling of asperities on slip, for predicting strong ground motion by only analyzing observed data of past earthquakes. On the other hand, through numerical simulations of fault rupture dynamics, it is possible to obtain important information on the type of final slip distribution that can occur in a stress state before the occurrence of multiple earthquakes by performing parametric analysis on specific relationships. However, the range of fault rupture parameters to be used in the parametric studies should be physically valid and constrained by empirical relationships.

As a joint research between LLNL and DPRI on the rupture dynamics for crustal earthquakes, we carried out analyses on the effects of several dynamic rupture parameters on the fault, such as stress drop, slip weakening distance, and strength excess on final fault slip, slip velocity, and rupture speed. In addition, we examined potential relationships between the assumed initial stress conditions, including asperities location, and rupture initiation time and the final slip and slip velocity obtained from the spontaneous rupture modeling.

## 2. Method of Analysis

Here, we describe the basic features of the finite-difference method for modeling the rupture dynamics used in Pitarka et al. (2009) [1], which is based on the method proposed by Dalguer and Day (2007) [2]. In the formulation of Dalguer and Day (2007) [2], two nodes (so-called split-node) are placed at the same position on the fault plane, and the continuity conditions of the equilibrium of forces and displacement between the two points are considered. The differential scheme involves a staggered grid finite difference method for velocity and stress. The setting of the shear stress boundary conditions on the fault plane is carried out according to the following equation.

$$\tau_c - \tau \geq 0 \quad (1)$$

$$\tau_c \dot{\mathbf{s}} - \tau \dot{\mathbf{s}} = 0. \quad (2)$$

Here,  $\tau$  is the shear stress acting on the fault plane,  $\mathbf{s}$  is the slip vector, and  $\tau_c$  represents the shear strength of the plane. Equation (2) shows the equilibrium of out-of-plane forces. The equation of motion at the fault plane for the split-nodes ( $\pm$ ) is expressed as below.



$$\rho_{j,k}^{\pm} \left\{ \frac{[u_x^{\pm}(t + \Delta t/2)]_{j,k} - [u_x^{\pm}(t - \Delta t/2)]_{j,k}}{\Delta t} \right\} = \frac{[D_x^{(2)} \sigma_{xx}^{\pm}(t)]_{j,k} + [D_y^{(2)} \sigma_{xy}^{\pm}(t)]_{j,k} \pm 2 \left\{ [\sigma_{xz}(t)]_{j,k, l_0 \pm 1/2} - [T_x(t) - T_x^0]_{j,k} \right\}}{\Delta x} \quad (3)$$

Here, the left-hand side is the acceleration times the mean density at time  $t$  at point  $(j, k)$ , and the right-hand side is the spatial derivative of the stress on the fault plane.  $T$  is the shear traction on the fault plane, and  $T^0$  is the initial value.  $D_i$  is the differential operator. By solving this equation with the finite difference method, the amount of slip on the fault plane is obtained.

As a constitutive relationship at the fault surface in the studies of Dalguer and Day (2007) [2] and Pitarka et al. (2009) [1], the simple slip weakening model of Andrew (1976) [3] is used, which is shown in Fig. 1. The symbols used here are:

- $\sigma_u$  : maximum stress (strength)
- $\sigma_0$  : initial stress
- $\sigma_r$  : residual stress
- $T_u$  : breakdown strength drop
- $T_e$  : dynamic stress drop (=static stress drop)
- $D_c$  : critical slip weakening distance

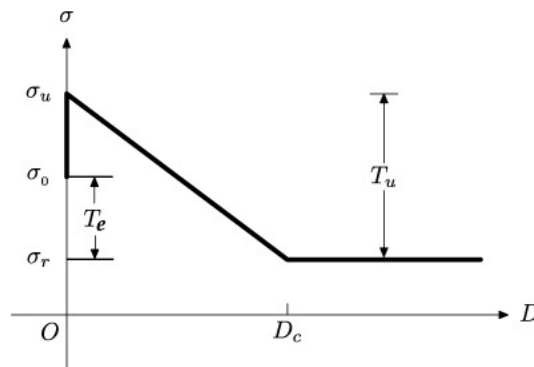


Fig. 1 – Slip-weakening model of Andrew [3] used in the study.

The advantage of using a linear slip weakening friction law is that the modeler can directly impose the expected amounts of dynamic stress drop and strength excess out of the spontaneous rupture model, without necessarily using absolute values of the initial normal and shear stresses as inputs. Dalguer and Day (2007) [2] verified the convergence of numerical resolutions comparing the resulting time histories of the stress and slip velocity functions for two different grid sizes (namely 100m and 300m) with the highest resolution model of 50 m grid size. Although there is little difference between the results of the 300 m grid-size case and that of the highest resolution, there is almost no difference between the results of the 100 m grid-size case and that of the highest resolution.

Then by using spontaneous rupture simulations for M6.9-7.3 crustal earthquakes, Pitarka et al. (2009) [1] examined how the frequency content of computed strong motion characteristics depends on whether the



rupture crosses the entire weak zone and reaches the free surface. In their stress model the stress drop on the fault plane and shear and normal stresses were spatially varied using a stochastic scheme. The spatial variation of stress drop follows the  $k^{-2}$  model of Mai and Beroza (2002) [4] in the slip distribution derived from the analysis of empirical data of the inverted spatial slip distributions. The average stress drop is set to 5 MPa, and the amount of stress drop near the surface as well as the bottom is reduced so that the amount of slip gradually decreases in the upper 5 km of the top of the fault rupture and the bottom 3 km of the fault below 15 km. The value of the critical slip weakening distance  $D_c$  is gradually increased in both top and bottom parts of the fault.

In Pitarka et al. (2009) [1] three different stress drop distributions were considered in which the reduction rate of stress drop in the shallow portion of the fault is varied in order to produce three distinct rupture scenarios. In the first scenario with a gentle reduction rate the fault rupture reaches the surface, and the resulting ground displacement is substantial. In the second scenario with a moderate reduction rate the rupture reaches the surface, but the resulting ground displacement is very small. In the third scenario with zero stress drop near the surface, representing buried fault earthquakes, the rupture does not reach the free surface. The effects of the weak zone on rupture dynamics, as well as shallow slips and near-fault ground motions are quite significant. The peak ground velocity is higher for buried ruptures and lower when rupture reaches the free surface. This correlation is reversed for the near-fault ground motion displacement and long-period ground motion velocity.

By referring to these previous studies we conducted parametric studies focusing on the dynamic fault parameters, especially the depth dependence of them, to delineate their influence on the slip distribution on the fault surface and the resulting ground velocity levels. The major difference of our simulation to the previous studies is that we introduce a couple of rectangular high-stress drop patches that correspond to the asperities (or Strong Motion Generation Areas, SMGAs) delineated from the kinematic rupture process inversions (e.g., Irikura and Miyake, 2011 [5]).

### 3. Results

#### 3.1 Stress Drop Model

In our analysis of the effects of dynamic rupture parameters on simulated rupture kinematics and near-fault ground motions we focused on the following rupture model parameters: a) the asperity depth, b) the rupture initiation point, c) the slip weakening distance,  $D_c$ , d) the gradient that controls the stress drop near the ground surface.

The fault model used is an inland crustal earthquake equivalent to M6.7 with a maximum length of 25 km and a maximum width of 18 km, as a vertical strike-slip fault. Table 1 shows the one-dimensional ground structure used in the model. We assume a shallow bedrock structure of 5 km depth under a soft rock layer of 1 km thickness. We also assume a homogeneous half-space below 5 km.

Table 1 – One-dimensional crustal structure used in the simulation.

Layer	Depth(km)	Vp(km/s)	Vs(km/s)	density
1	0.5	1.2	0.68	2.1
2	1	1.9	1	2.2
3	5	4.8	2.8	2.4
4	Half Space	6	3.464	2.67

#### 3.2. Effects of asperity depth

Here we investigate the effects of asperity depth on computed final slip distribution. We used Irikura Recipe [5] for strong ground motion simulations to estimate the number and size of asperities (i.e., a patch with



elevated stress drop) expected for a M6.7 crustal earthquake. According to the recipe the number of asperities for a M6.7 earthquake should be two. Fig. 2 shows the dynamic fault rupture parameters used in rupture scenarios of Case 1, in which one deep asperity and one shallow asperity were included, and Case 2, in which both asperities are shallow. The top left, top right, middle left, middle right and the bottom left of each figure show the shear stress, normal stress, and stress drop, strength excess distributions, and critical slip-weakening distance  $D_c$ , respectively. Except for  $D_c$ , random spatial variations of stress parameters were imposed simultaneously. The random spatial variation follows the  $k^{-1}$  model in stress derived from the  $k^{-2}$  model in slip of Mai and Beroza (2002) [4].

Fig. 3 shows the comparison of computed final slip and spontaneous rupture time between the deep (Case 1) and shallow (Case 2) asperities rupture scenarios. As seen in this figure, when one of the asperities is deep, the resulting slip distribution follows the asperity locations. In contrast, when both asperities are shallow, because of the rupture interaction with the free surface, the resultant slip is more homogeneous and uniformly distributed in the asperity areas. The deep asperity does not contribute so much to the near-surface slip.

Next, we generated a suite of 120 rupture realizations for which the small asperity remained fixed in its original position, as shown in Fig. 2, while the large asperity was randomly located at different depths starting from shallow (2-6 km), intermediate (6-8km) to deep (8-10 km). The result of the simulations in terms of maximum and average slip, and maximum and average ground motion velocity on the surface is shown in Fig. 4. It is important to note that the average slip is remarkably constant with a slight tendency to decrease with the asperity depth. The same tendency with a larger variation is observed in the maximum slip. The average and maximum peak ground velocity on the surface follows similar trends. However, the decrease in the maximum and average velocities with respect to the asperity depth is more than a factor of two, as opposed to only 25% decrease seen in the maximum slip.

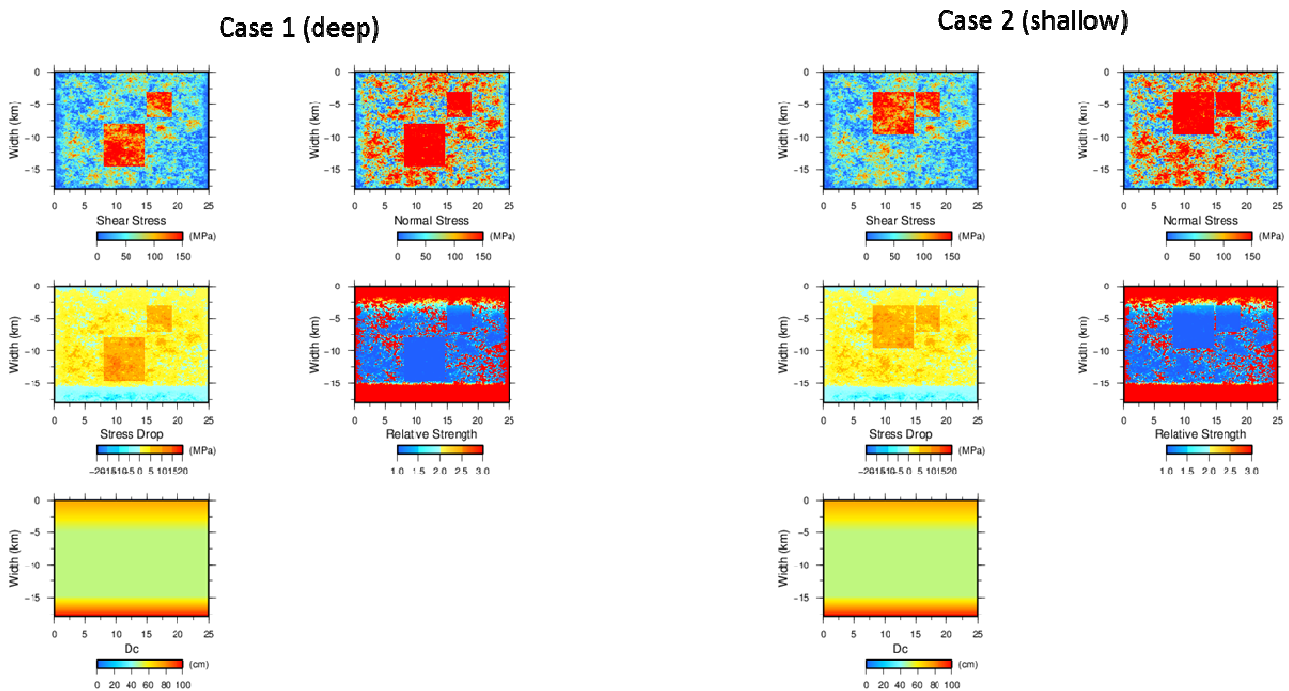


Fig. 2 – Parameters for deep (Case 1) and shallow (Case 2) asperity scenarios.



Case 1 (deep asperity)

Case 2 (shallow asperity)

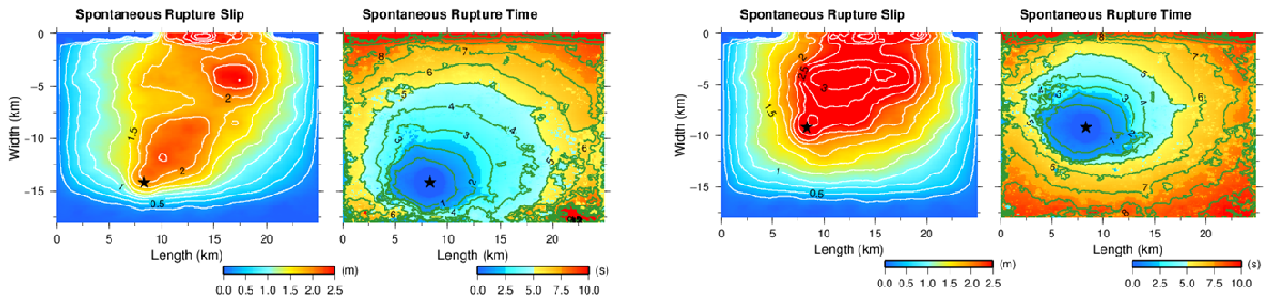


Fig. 3 – Comparison of slip amount and rupture initiation time between deep and shallow asperity scenarios shown in Fig.2.

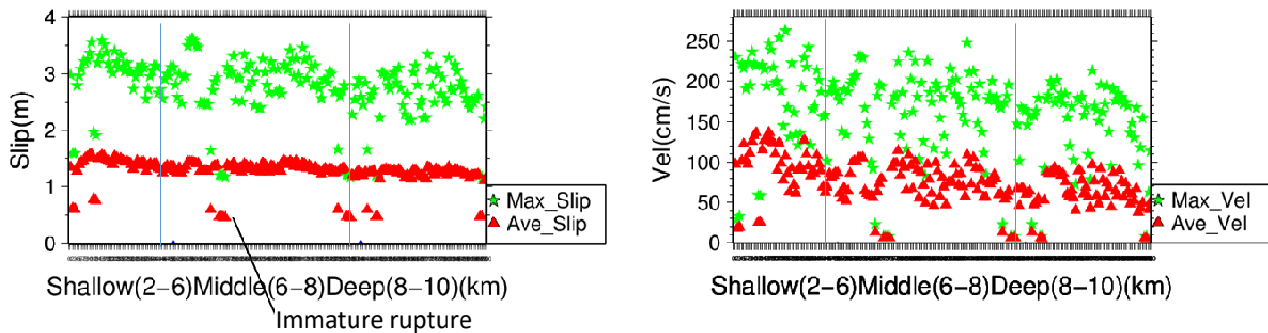


Fig. 4 – Fluctuations in the maximum and average slip amount (left) and the maximum and average peak ground velocity (right) due to variations in the larger asperity depths. The horizontal axis corresponds to the larger asperity depth.

### 3.3 Effects of distance between asperities

Here we investigate the effects of inter-asperities distance on the simulated final slip and the near-fault surface peak ground velocity. Fig. 5 shows the dynamic fault rupture parameters for the rupture scenario Case 1, in which the small and large asperities are located next to each other, and Case 2 in which the two asperities are separated by 4 km. The resulting distributions of the final slip and the spontaneous rupture time are shown in Fig. 6 as before.

The two asperities close to each other in Case 1 act as a single asperity. The corresponding large slip area is larger than the large slip area obtained for Case 2 where the asperities are well separated. Most importantly, the second model produces smaller fault surface slips and lower peak ground velocities.

Fig. 7 shows variations of computed fault slip and near-fault surface ground motion velocity as a function of the inter-asperity distance. We use 120 rupture scenarios for which the inter-asperity distance randomly varies between 0 to 4.7 km. We should note that the average slip is practically independent of the inter-asperity distance. This could be so probably because the separation between two asperities is relatively small compared to the size of the largest asperity in all 120 scenarios. On the other hand, the resultant peak ground motion velocity is sensitive to the inter-asperity distance and varies by more than a factor of two between the scenarios. Being representative of higher frequency ground motion the near-fault peak ground velocity is sensitive to the local directivity effects and interactions between the local rupture dynamics and the free surface.

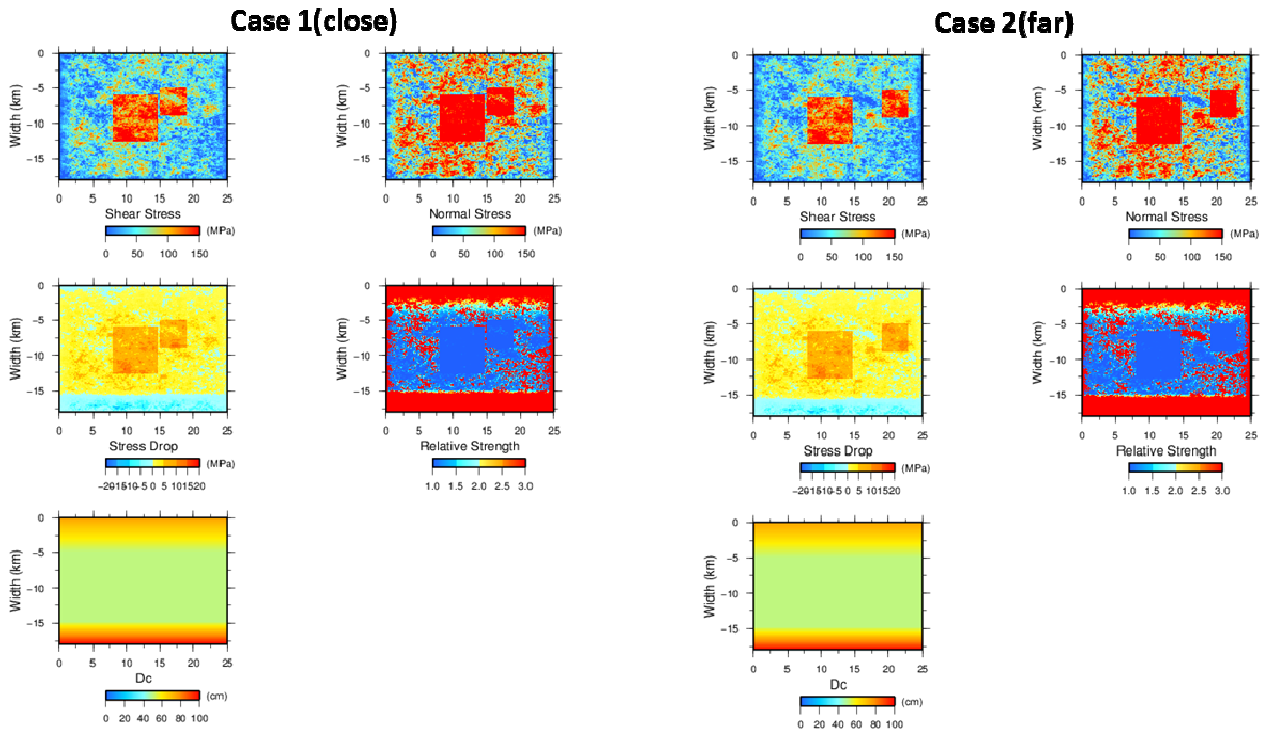


Fig. 5 – Parameters for close asperity scenario (Case 1) and far asperity scenario (Case 2).

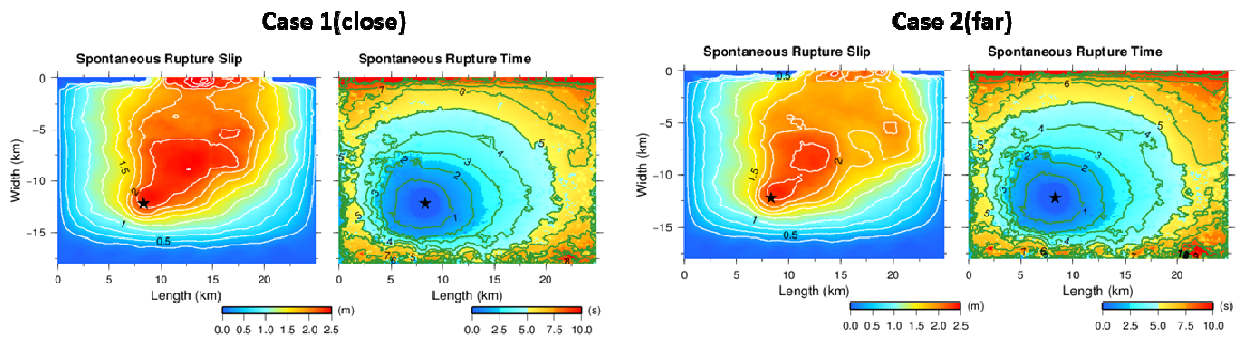


Fig. 6 – Resultant effects of asperity distance on slip distribution and rupture initiation time.

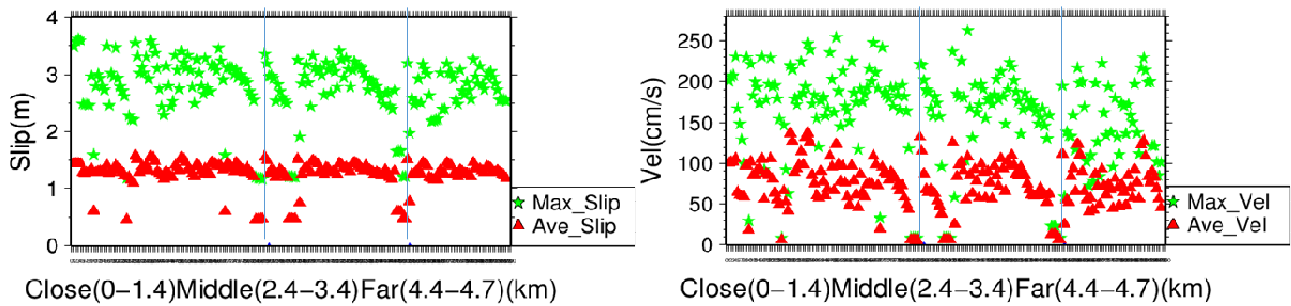


Fig. 7 – Fluctuations in the maximum and average slip amount (left) and the maximum and average peak ground velocity (right) due to variations in the inter-asperity distance. Horizontal axis corresponds to inter-asperity distance



### 3.4 Effects of rupture initiation point

In all rupture scenarios described above the rupture initiates in the lower-left corner of the large asperity. This particular location favors upward directivity effects and in the case of shallow asperities favors along-strike directivity effects, too. The rupture initiation location should have a significant impact on the overall spontaneous rupture process. We investigated its influence on the results of slip and ground velocity. Fig. 8 illustrate two rupture scenarios with identical parameters except for the rupture initiation location. In Case 1 the rupture starts from the lower corner, while in Case 2 it starts from the upper corner of the large asperity.

The slip and rupture time distributions resulting from each scenario are shown in Fig. 9. There is a significant difference in slip and rupture time distributions between the two scenarios. It shows that rupture initiation controls the effects of local rupture directivity. As indicated by the simulation results shown in Fig. 10, there are large fluctuations in both slip and peak ground motion velocity due to the depths of the rupture initiation points. This variability does not necessarily correlate with the rupture initiation depth since the effect of rupture directivity, as well as spontaneous rupture propagation speed, depend on the relative location of asperity areas with respect to the rupture initiation location and proximity to the free surface.

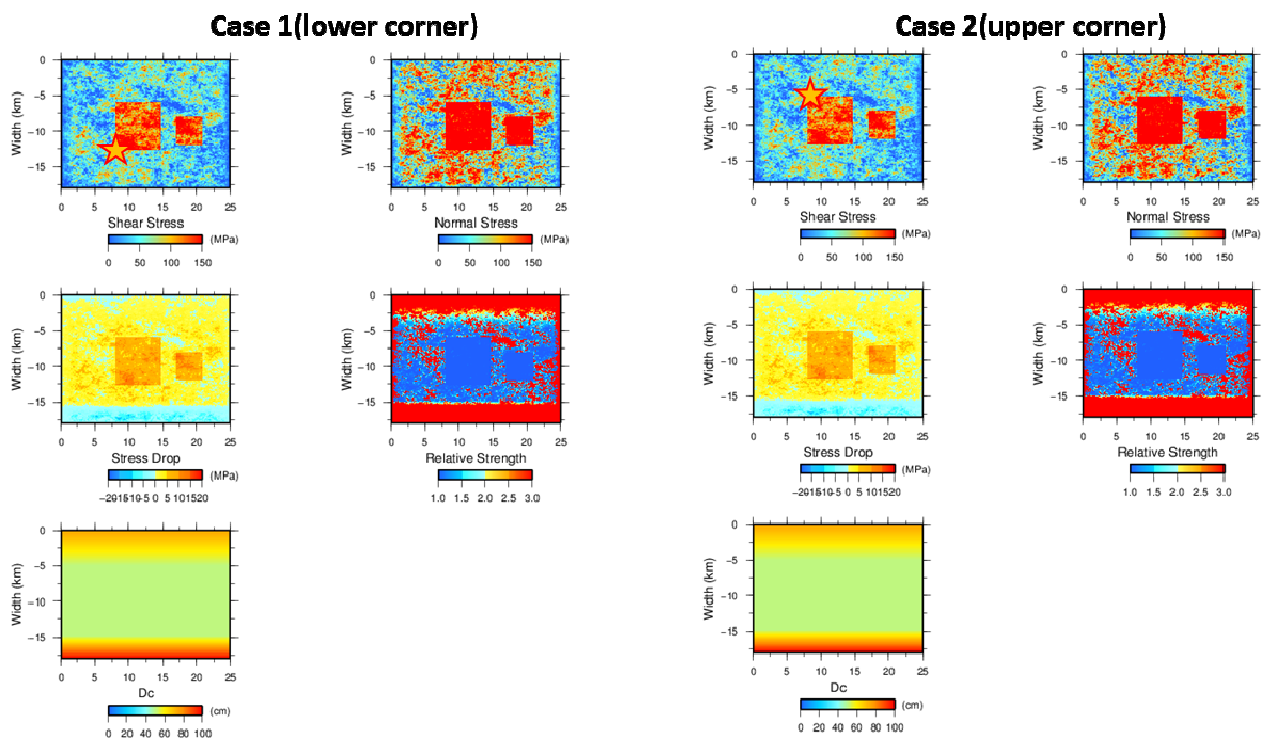


Fig. 8 – Deep initiation point (☆) scenario (Case 1) and shallow initiation point scenario (Case 2).

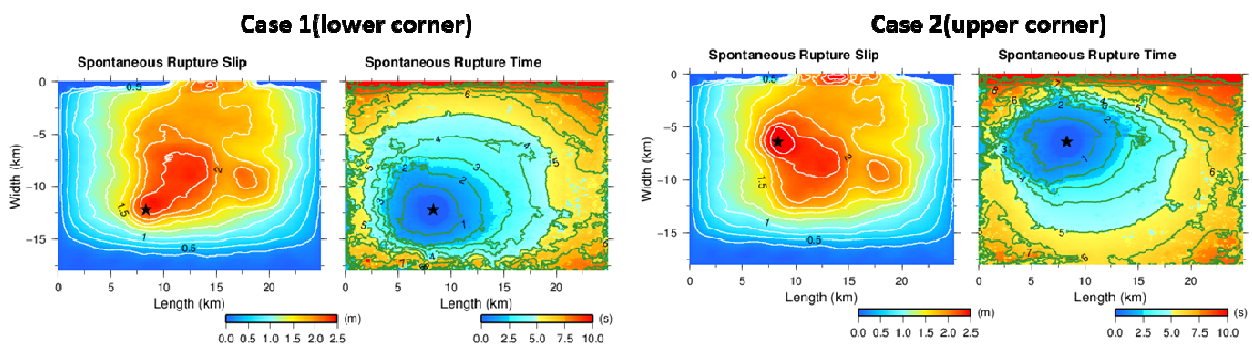


Fig. 9 – Resultant effects of rupture initiation point on slip distribution and rupture initiation time.

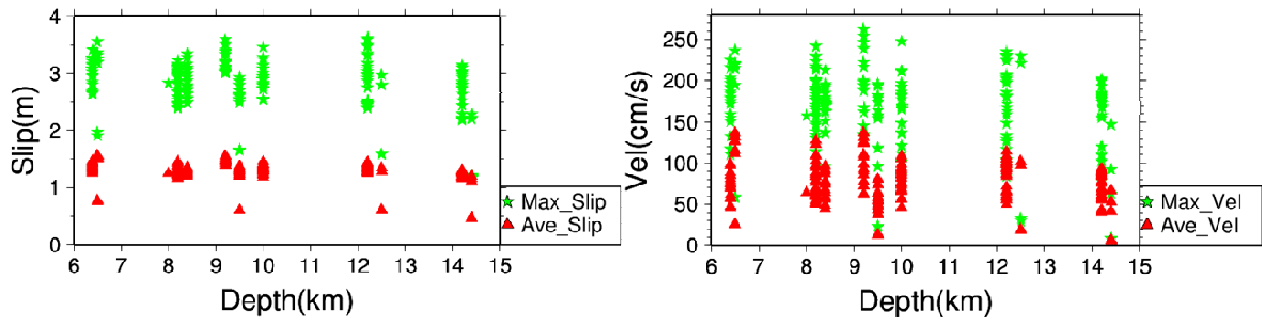


Fig. 10 – Fluctuations in the maximum and average slip amount (left) and the maximum and average peak ground velocity (right) due to variations in the depth of the rupture initiation point.

### 3.5 Effects of $D_c$

The critical slip-weakening distance  $D_c$  controls the fracture energy. A larger  $D_c$  increases the energy consumed by the fracture. Consequently, a larger  $D_c$  suppresses the advancement of fracture because a larger energy is required by the fracture to propagate. Relatively speaking, large  $D_c$  slows down the rupture, while small  $D_c$  increases the rupture propagation speed, and consequently increases the slip velocity. Since  $D_c$  trades off with stress drop, its effect on rupture propagation also depends on the assumed overall stress distribution on the fault. In our rupture models the  $D_c$  is set to 50 cm in the seismogenic zone (depths range 5-15km) and it linearly increases at depths shallower than 5km and deeper than 15km. In our models  $D_c$  at the ground surface is set to 75 cm, and 100 cm at 18km. We investigated the effects of  $D_c$  assigned to the seismogenic zone on rupture dynamics by performing simulations with three different models with different  $D_c$ , Case 1, Case2, Case3, for which  $D_c$  is 50cm, 52cm and 55cm, respectively. Fig. 11 shows the stress models and Fig. 12 shows the results of rupture dynamics simulations. In Case 3 where  $D_c=55$  cm the rupture stops as soon as it starts. Decreasing  $D_c$  from 52cm to 50 cm increases the rupture speed and slightly increases the free surface slip. Based on the similar analysis of  $D_c$ , most of our stress models have a  $D_c$  with a base value of 50 cm which produces a sub-shear rupture propagation.

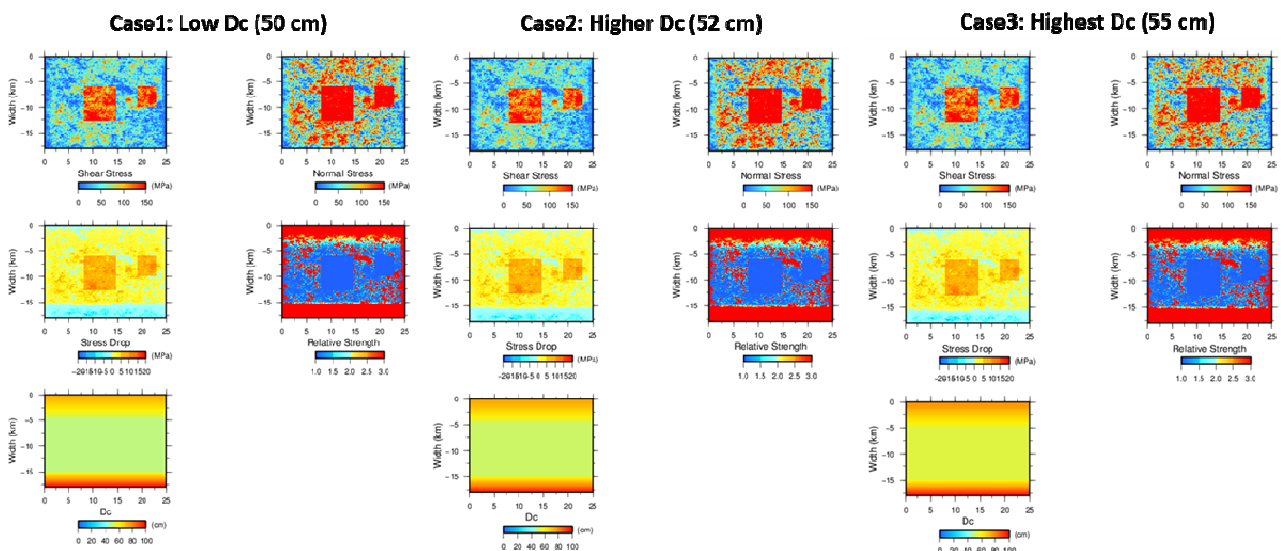


Fig. 11 – Source parameters of small  $D_c$  (Case 1), slightly larger  $D_c$  (Case 2), and large  $D_c$  (Case 3).

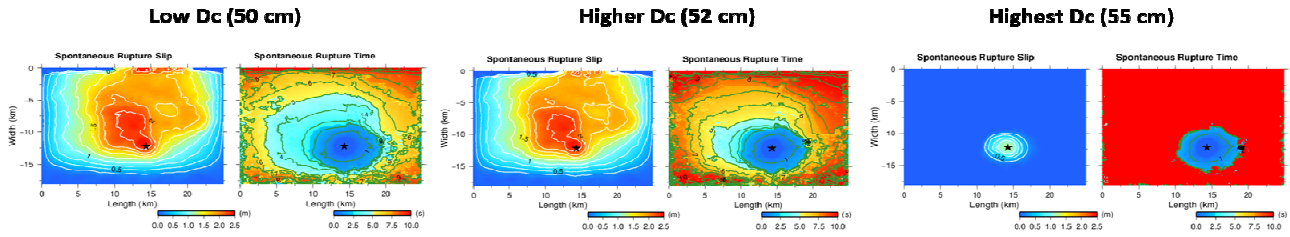


Fig. 12 – Comparison of slip and rupture initiation time for three cases with different Dc values.

### 3.6 Effects of stress drop gradient near the surface

Here we investigate the effect of near-surface stress drop on simulated rupture dynamics and near-fault ground motion. As explained earlier, we included a weak zone in which stress drop is set to zero or negative at the free surface and linearly increases with depth in the top 5 km of the crust. In this study the average stress drop at 5km depth was set to 3.2 MPa. We considered two stress models. In Case 1 model, the near-surface stress-drop gradient is 0.06MPa/km which yields a zero stress drop at the free surface. In Case 2 model, the gradient was 0.064MPa/km which yield a negative stress drop at the free surface (Fig. 13).

Fig. 14 shows the simulated final slip and rupture time distributions for Case 1 and Case 2 models. The slip distribution shows that the near-surface slip is very sensitive to the stress drop in the shallow part of the crust. A weaker near-surface zone (smaller stress drop zone with large Dc) limits the surface rupture to a smaller portion of the fault. When we inspected the maximum and average slip, and maximum and average ground motion velocity for several cases with different stress drop gradient to the surface, we found that the maximum slip (concentrated along the free surface) decreases with decreasing near-surface stress drop. The effect is drastic on ground motion amplitudes; peak velocity increases by a factor of 3 when near-surface stress drop increases from a negative value to zero.

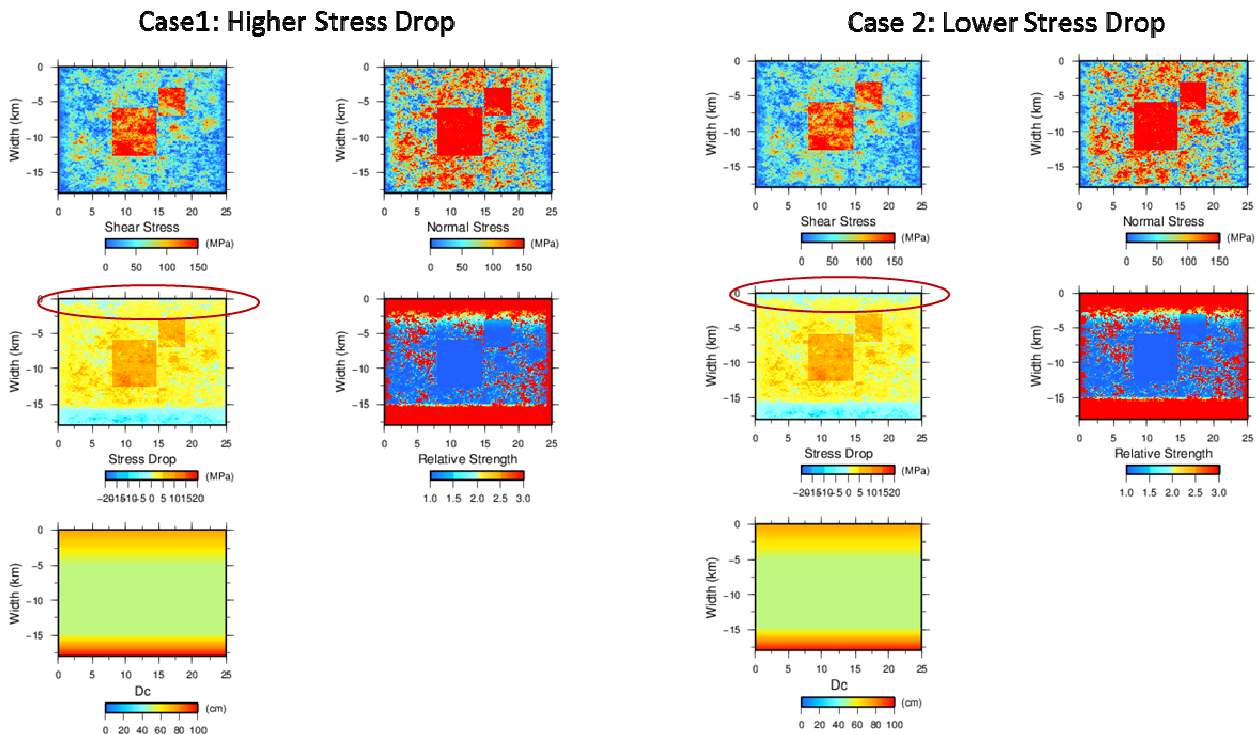


Fig. 13 – The case where the stress drop near the surface is almost zero (Case 1), and the case where it is a negative value (Case 2)

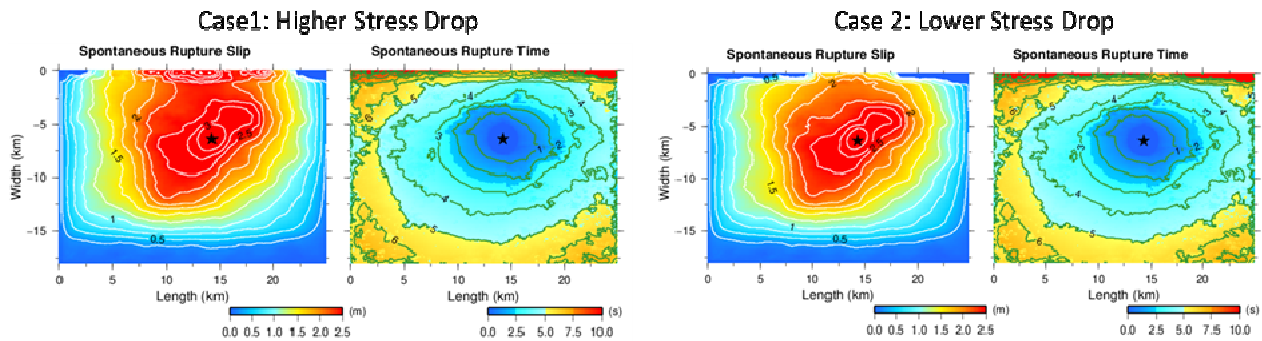


Fig. 14 – Resultant effects of the stress drop near the surface on slip distribution and rupture initiation time.

#### 4. Summary and Conclusions

In our analysis of effects of dynamic rupture parameters on simulated distributions of slips on the fault and near-fault ground motions, we focused on the following rupture model parameters: a) the asperity depth, b) the inter-asperity distance, c) the rupture initiation point, d) the slip weakening distance  $D_c$ , and e) the near-surface stress drop. The conclusions drawn from our numerical experiments are as follows:

##### 1) Effects of asperity depth:

Shallower asperities generate larger mean and maximum fault slip, as well as larger near-fault ground motion velocity. The mean and maximum ground surface velocity follow similar trends. However, the decrease in maximum peak and average velocities with asperity depth is more than a factor of two, as opposed to only 25% decrease in the maximum slip.

##### 2) Effects of inter-asperity distance:

The average slip is practically independent of the inter-asperity distance. This could be so probably because the separation between the asperities is relatively small compared to the size of the largest asperity. In contrast, ground motion velocity is sensitive to the inter-asperity distance (local cumulative rupture directivity) and varies by more than a factor of two between the scenarios. Being affected by high-frequency ground motion the near-fault peak ground motion velocity is sensitive to the local directivity effects and local interactions between local rupture dynamics and the free surface.

##### 3) Effects of location of rupture initiation point:

The rupture initiation location controls local rupture directivity. As indicated by the simulation results shown in Figure 9, there is a large variation in both slip and peak ground motion velocity. The variability does not necessarily correlate with the rupture initiation depth, since the effect of rupture directivity, as well as spontaneous rupture propagation speed, depends on the relative location of asperity areas with respect to the rupture initiation location and proximity to the free surface.

##### 4) Effects of critical slip-weakening distance $D_c$ :

It was found that critical slip-weakening distance  $D_c$  has little effect on mean and maximum slip amounts. However, if  $D_c$  is too large, it causes immature fracture, while large  $D_c$  results in small mean and maximum ground surface velocity.

##### 5) Effects of near-surface stress drop:

The slip distribution shows that the near-surface slip is very sensitive to the stress drop in the shallow part of the crust. A weaker near-surface zone (smaller stress drop and large  $D_c$ ) limits the surface rupture to a smaller portion of the fault. We found that the maximum slip (concentrated along the free surface) decreases



with decreasing near-surface stress drop. The effect is drastic on ground motion amplitudes. Peak velocity increases by a factor of 3 when near-surface stress drop increases from a negative value to zero.

Based on these results, the following investigations are necessary in future studies:

- Perform calculations for a uniform, semi-infinite half-space, which means that we assume no low-velocity layers near the surface. A soft material near the surface used here is likely to have significant effects.
- Perform calculations for earthquakes with larger magnitude. In this study we only investigated rupture models for an intermediate-size earthquake of M6.7.
- Investigate how much effects will be manifested when the dependency of stress drop with depth in the seismogenic zone is considered as seen in Nakano et al., (2015) [6].
- Examine whether the scaling law of asperity derived by characterizing the obtained slip distributions from the method for kinematic inversions [5] agrees with that from the dynamic rupture simulations.
- Obtain ground motion prediction equation (GMPE) from simulated velocity waveforms and compare it with empirical GMPEs.

## 5. Acknowledgment

A part of the analyses shown here were performed by Atsundo Manpo when he was a graduate student in the School of Engineering, Kyoto University. A part of the study was supported by the JSPS Kakenhi Grant-in-Aid for Basic Research (B) No.19H02405.

## References

- [1] Pitarka, A., L.A. Dalguer, S.M. Day, P.G. Somerville, and K. Dan (2009): Numerical Study of Ground-Motion Differences between Buried-Rupturing and Surface-Rupturing Earthquakes, *Bull. Seismo. Soc. Am.*, Vol. 99, No. 3, 1521-1537, doi: 10.1785/0120080193.
- [2] Dalguer, L.A., and S. M. Day (2007): Staggered-grid split nodes method for spontaneous rupture simulation, *J. Geophys. Res.* 112, B02302, doi: 10.1029/2006JB004467.
- [3] Andrew, D.J., (1976): Rupture velocity of plane-strain shear cracks, *J. Geophys. Res.* 81, 5679-5687.
- [4] Mai, P.M., and G.C. Beroza (2002): A spatial random field model to characterize complexity in earthquake slip, *J. Geophys. Res.*, 107, No. B11, 2308, doi: 10.1029/2001JB000588.
- [5] Irikura, K. and H. Miyake (2011): Recipe for predicting strong ground motion from crustal earthquake scenarios, *Pure Appl. Geophysics*, 168, pp.85-104.
- [6] Nakano, K., S. Matsushima, and H. Kawase (2015): Statistical properties of strong ground motions from the generalized spectral inversion of data observed by K-NET, KiK-net, and the JMA Shindokey Network in Japan, *Bull. Seism. Soc. Am.*, 105: 2662-2680, doi:10.1785/0120140349.